

Optical Flow and Scale-Space Theory applied to Sea-Ice Motion Estimation in Antarctica

Salvador Gutiérrez and David G. Long
Microwave Earth Remote Sensing Laboratory
Brigham Young University
459 Clyde Building, Provo, UT 84602

Email: salvador@et.byu.edu, long@ee.byu.edu Fax: (801) 422-0201

Abstract—Sea-ice motion in Antarctica is studied applying methods from computer vision and scale-space theory to a sequence of images obtained from scatterometer data. The proposed method can obtain a dense motion vector field for any specific observation scale. Spatial and temporal scales are used to focus on relevant geophysical features and events.

A preprocessing stage involving spatial and temporal filtering at selected scales reduces noise and artifacts produced in the image generation phases, allowing reliable feature extraction and tracking at relevant scales. Optical flow (OF) methods provide a dense estimation of the motion field. The limitations and advantages of this approach are discussed. Optical flow sea-ice motion data are in agreement with sea winds data obtained independently and with very different methodologies. OF results are compared to data from wavelet methods.

I. INTRODUCTION

The problem of determining sea-ice directions and speeds on Antarctica has been previously approached with correlation [1] or wavelet [2], [3] based methods. These methods result in *sparse* vector fields of sea-ice velocities. A new approach based on techniques borrowed from computer vision has been developed to produce *dense* vector fields.

These methods are applied to QuikSCAT imagery, after being processed with a resolution-enhancing algorithm [4] and ice-masked.

II. SCALE

The measurement of an observable variable has an associated aperture in space and time, which defines its effective spatial and temporal resolution. While some physical phenomena appear the same at different scales (e.g., fractal objects), most phenomena do not exhibit such scale invariance. Defining the appropriate scales (spatial and temporal) used in the measurement process is as important as defining a reference frame. It should be considered, however, that due to aperture averaging, features of size less than the corresponding scale cannot be observed.

III. DATA PREPARATION AND PREPROCESSING

QuikSCAT ice-masked imagery represents values of σ^o from the scatterometer which have been corrected, combined and integrated to cover the whole continent of Antarctica, producing an intensity image of σ^o . The intensity function for each image $I : \mathbb{R}^2 \rightarrow \mathbb{R}$ is defined for almost the whole continent, save for a small area around the pole not covered by

satellite swaths. Outside of the continent the intensity function is defined only for points corresponding to sea-ice, and left undefined for areas corresponding to open ocean. Ice masking is done as a separate pre-processing step.

A sequence of n images corresponding to consecutive days can be represented as an array $I^{(t)}(x, y)$ where $x, y \in \mathbb{Z}_+$ correspond to pixel positions and $t \in T = [d_1, \dots, d_n]$ is the index of each image in the sequence. Time filtering is the convolution of a one-dimensional kernel, taken here to be a gaussian, with the sequence of intensity values corresponding to each pixel

$$\tilde{I}^{(t)}(x, y) = g(0, \sigma^2) \star I^{(t)}(x, y).$$

IV. DIFFERENTIAL INVARIANTS AND FEATURES IN SCALE-SPACE

The scale-space representation used in the images reported in this paper is a multi-scale representation with a continuous scale parameter, [5], [6]. This scale space roughly consists of convolutions of the image with gaussian low pass filters. The scale parameter is related to the kernel's effective length for the particular filters used. The same idea applies to the temporal scale.

A faithful edge-finder is expressed by the conditions $I_{vv} = 0$ and $I_{vvv} < 0$ at any point P_0 . This invariant may be interpreted as the maximum of the gradient in the direction of the gradient. When computed with derivatives defined at different scales this invariant results in a scale-space of edges that more faithfully follow the contours of geophysical features. Most of the observed displacements of the edge-like features described in this section, lie within the range of 0 to 10 km (0 to 2.25 pixels) between consecutive frames (see Fig 1). Events lasting less than 1.5 days are filtered out by time-smoothing.

V. OPTICAL FLOW (OF) METHODS

The key relationship in these methods, usually referred to as Horn's restrictive equation [7], can be derived from the assumption that the intensity and shape of a moving neighborhood on the observed object remain invariant in a short interval. Horn's restrictive equation can be written as a total derivative of an intensity function

$$\frac{dI}{dt} = \frac{\partial I}{\partial x} \frac{dx}{dt} + \frac{\partial I}{\partial y} \frac{dy}{dt} + \frac{dI}{dt} = \nabla_s I \cdot \mathbf{u} + I_t = 0 \quad (1)$$

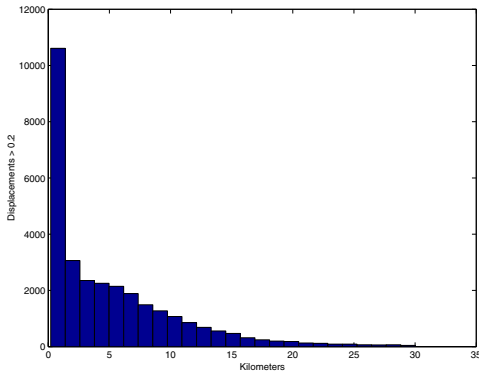


Fig. 1. Distribution of sea-ice displacements found by the OF method. Antarctica, JD 277, 1999 (in kilometers). Displacements less than 0.2 km have been removed to facilitate appreciation of detailed distribution structure.

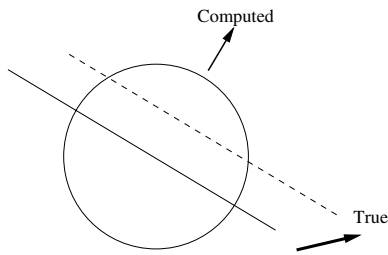


Fig. 2. The aperture problem in a neighborhood based method, only the motion component in the direction of the gradient can be determined without ambiguity.

where $\mathbf{u} \equiv \left(\frac{dx}{dt}, \frac{dy}{dt} \right)^T$, $I_t \equiv \frac{d}{dt}I$ and s is the scale parameter. The derivatives $\frac{\partial I}{\partial x}$, $\frac{\partial I}{\partial y}$ and $\frac{d}{dt}I$ are computed by convolution with appropriate gaussian derivative kernels in space and time, leaving $\frac{dx}{dt}$ and $\frac{dy}{dt}$ as unknowns. This relation is underconstrained, since it is only one equation with two unknowns, although we may find a least-squares solution by taking points in a neighborhood. Only the optical flow component in the direction of the gradient can be determined, a problem known as the *aperture* problem (see Fig. 2).

This is one of the main limitations of OF methods. The basic relation can be further constrained in many ways. We follow the approach explained in [8], which imposes a second order constraint by observing that if $\frac{D}{dt}I$ vanishes, then higher order total derivatives must also vanish. In particular, $\frac{d^2}{dt^2}I = 0$ which implies that $\frac{\partial}{\partial t} \nabla I \cdot \mathbf{u} + \nabla I \cdot \frac{\partial}{\partial t} \mathbf{u} + \frac{\partial^2}{\partial t^2}I = 0$.

When $\frac{\partial}{\partial t} \mathbf{u} \rightarrow 0$ and $\frac{\partial^2}{\partial t^2}I \rightarrow 0$, these relations for each pixel in a certain neighborhood, give a system of equations whose least squares solution yields the OF. Generally, regularizing the field is desirable. It is possible to regularize the field by computing the least squares solution with bigger neighborhoods (in this paper we used a circular neighborhood with a diameter of 30 pixels). Using relatively large neighborhoods to find the least squares solution regularizes the direction of the OF, which is desirable, but results in smaller magnitudes because more points contributing in different directions are

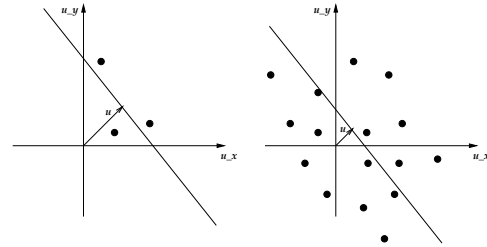


Fig. 3. Left. Taking points from a neighborhood leads to an overdetermined system that has a least squares solution. Right. Taking bigger neighborhoods regularizes the directions of the vector field (alleviating the aperture problem), but may lead to smaller magnitudes of vector \mathbf{u} , because more points contributing in different directions will be included.

TABLE I

ERROR BETWEEN WAVELET AND OF ESTIMATES OF MOTION VELOCITY.

	JD 271	JD 277	JD 277
Neighborhood radius	15px	15px	60px
AEE (pixels/day)	4.01	3.71	3.70
AAD (degrees)	59.48°	64.28°	58.65°
RMS (pixels/day)	4.96	4.35	4.46
Number of points	1,120	1,108	1,108

included, bringing the estimated line closer to the origin, thus decreasing the magnitude of \mathbf{u} (see Fig. 3). In other words, uncertainty in the magnitude of the displacement is traded for a more robust estimator of the motion direction, in fact, reducing the aperture problem.

A correction factor for the magnitudes can be found through various means. A reasonable estimate is the ratio of the maximum detectable displacement to the maximum detected displacement, the former quantity is just the neighborhood size whereas the latter is easily found from the computed displacements.

VI. RESULTS AND VALIDATION

Data from sea-ice motion using the wavelet method [9] were compared to the OF data using three different measures of error: The average euclidean error (AEE), the average angular difference (AAD), and the root mean square error (RMS).

The shape of the sea ice displacements distribution from OF (Fig. 1) does not match the shape of the corresponding distribution obtained using the wavelet approach (Fig. 4), the distribution of the OF data is closer to intuition, having the smaller displacements being the most frequent.

Magnitudes of the wavelet data are consistently larger than those of the OF data, although the OF data are more in agreement with the observed displacement of linear features (see Fig.6). The differences in direction diminish when the scale is augmented (as seen in Table I), but cannot be completely explained by differences in scale alone. Local analysis show that there are some regions where both data sets agree very closely in direction, and some others where the differences are big, but so far no explanation could be found.

The results from optical flow estimation are consistent with the observed displacement of the curvilinear features, which

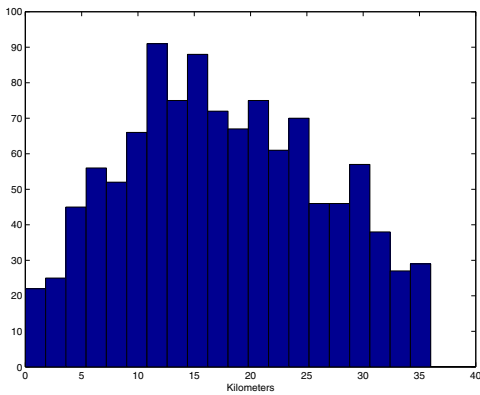


Fig. 4. Distribution of sea-ice displacements found by the wavelet method. Antarctica, JD 277, 1999 (in kilometers).

are a very reliable reference frame because they appear where there is a maximum amount of image information.

VII. CONCLUSION

OF methods can be successfully applied to estimate sea-ice motion from data from scatterometers such as SeaWinds on QuikSCAT. Dense motion vector fields can be obtained for selected scales, after appropriate pre-processing. Differential invariants can be used to find features on any scale and these features can be tracked. Results from OF agree with ocean surface wind data. Further work remains to be done in deriving adequate physical models that can further constrain the OF methods and refine their results.

REFERENCES

- [1] W. Emery, C. Fowler, and J. Maslanik, "Satellite-derived maps of Arctic and Antarctic sea ice motion: 1988 to 1994," *Geophysical Research Letters*, vol. 24, no. 8, pp. 897–900, 1997.
- [2] A. Liu, Y. Zhao, and S. Wu, "Arctic sea ice drift from wavelet analysis of NSCAT and special sensor microwave imager data," *Journal of Geophysical Research*, vol. 104, pp. 11 529–11 538, 1999.
- [3] A. Liu and D. Cavalieri, "On sea ice drift from the wavelet analysis of the defense meteorological satellite program (DMSP) special sensor microwave imager (SSM/I) data," *International Journal of Remote Sensing*, vol. 19, no. 7, pp. 1415–1423, 1998.
- [4] D. S. Early and D. G. Long, "Image reconstruction and enhanced resolution imaging from irregular samples," *IEEE Transactions on Geoscience and Remote Sensing*, vol. 39, no. 2, pp. 291–302, Feb 2001.
- [5] B. M. ter Haar Romeny, Ed., *Geometry-Driven Diffusion in Computer Vision*. Dordrecht, The Netherlands: Kluwer Academic Publishers, 1994.
- [6] M. Nielsen, L. Florack, and R. Deriche, "Regularization and scale space," INRIA, Tech. Rep. 2352, Sep 1994.
- [7] B. K. P. Horn, *Robot Vision*. The MIT Press, 1986.
- [8] H. F. (Shekarforoush), "A closed-form solution for optical flow by imposing temporal constraints," in *IEEE International Conference on Image Processing*, vol. 3, 2001, pp. 656–659.
- [9] Y. Zhao, A. K. Liu, and D. G. Long, "Validation of Sea Ice motion from QuikSCAT with those from SSM/I and buoy," *IEEE Transactions on Geoscience and Remote Sensing*, vol. 40, no. 6, pp. 1241–1246, Jun 2002.

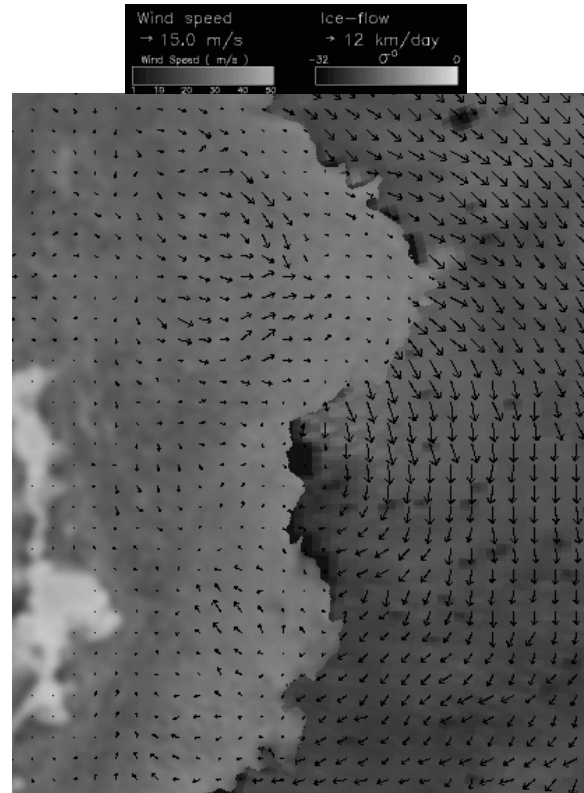


Fig. 5. This image combines the optical flow sea-ice motion data (left in light gray area) with ocean near-to-surface winds (to the right). The ice edge runs from top to bottom in the center of the image, the white area to the far left is due to ice shelves. Arrows over sea-ice are OF estimates; arrows over the ocean are JPL's QuikSCAT L3B sea winds data. The image shows a region to the East of the Davis Sea, in Eastern Antarctica, on Julian date 277, year 1999.

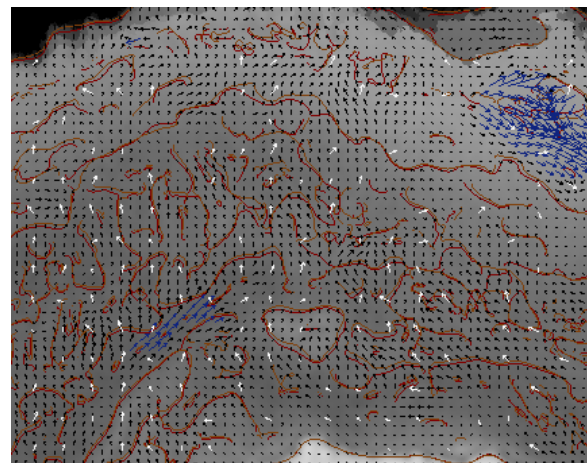


Fig. 6. OF estimation, overlaying a v-pol σ^0 image of the Weddell Sea. Vectors show OF estimates. Darker curves represent features of day 277, of year 1999, whereas the lighter ones correspond to day 278. White arrows are data from the wavelet method, gray arrows represent unreliable estimates.